AIAA Journal

VOLUME 8 AUGUST 1970 NUMBER 8

An Experiment on the MHD-Driven Rotating Flow for a Gas Core Nuclear Rocket

WENDELL L. LOVE* AND CHUL PARK†
NASA, Ames Research Center, Moffett Field, Calif.

A fluid dynamic simulation of a gas core nuclear rocket chamber has been made with the objective of separating a light and heavy gas by means of the centrifugal force produced by MHD-driven rotation. The test apparatus, a closed cylinder filled with a mixture of xenon and helium, uses a radial magnetic field configuration with an axial electric current passing between 16 pairs of electrodes. By observing the behavior of the discharge and the luminosity of the gas at different locations, the mode of discharge was found to be stable and suitable for effective separation. A rotating flow with transonic Mach number was produced as evidenced by the ratio (>2) of the pressure at the wall of the cylinder to that at the center. Spectroscopic measurements of the plasma condition show an appreciable degree of separation of the two species. The Hall parameter was found to be less than one.

Nomenclature

A = coefficient in temperature variation [Eqs. (A1) and (A2)]
B = radial magnetic field strength
c,cf = frozen speed of sound of gas mixture and of heavy species [Eq. (A10)], respectively
C = relative concentration of heavy species [Eq. (A9)]
D_{fp} = binary diffusion coefficient between light and heavy gas
D_f^T = thermal diffusion coefficient
F = expression defined by Eq. (A16)
J = electrical current
m_f,m_p = mass of heavy (i.e., fuel) and of light (i.e., propellant) gas atom, respectively
M = Mach number of gas mixture based on frozen speed of sound
M_{fa} = Mach number for heavy gas species based on frozen speed of sound [Eq. (A14)]
N = total particle number density, Eq. (A6b)
N_e = electron number density
$\bar{N}_f$ = total number density of the heavy gas atom and the heavy gas ion, Eq. (A6a)
N_f,N_p = number density of neutral heavy gas atoms and of light gas atoms, respectively
P = pressure
r = radial distance measured from centerline of chamber
R_1 = concentration ratio defined by Eq. (1)
R_2 = concentration ratio defined by Eq. (2)
T = temperature
u,v = radial and azimuthal gas velocity
μ = viscosity
ρ = density
θ = azimuthal angle
ω = electron cyclotron frequency
τ = electron collision time

Subscripts and superscripts

a = radial location of electrical discharge
f = heavy (i.e., fuel) gas
He = helium
J = current-only period of run
$J \times B$ = $J \times B$ period of run
o = centerline of cylinder
p = light (i.e., propellant) gas
w = wall of cylinder
Xe = xenon
$+$ = ion
$-$ = total, i.e., neutral plus ion, of one species

Received August 27, 1969; revision received January 28, 1970. The authors acknowledge and appreciate the contributions made by H. S. Friedman during the early period of the present work in which he participated.

* Research Scientist.

† Research Scientist. Member AIAA

Introduction

GASEOUS-CORE nuclear rocket engines offer the potential of high specific impulse combined with a large thrust-to-weight ratio. In order to realize this potential, however, it is necessary to minimize the loss rate of the gaseous nuclear fuel. A possible means for achieving this is described in the present study. In this scheme, the heavy nuclear fuel gas is retained near the wall of a cylindrical cavity by means of the centrifugal force produced by a rotating gas motion. The major portion of the light propellant gas flows axially along the centerline of the cavity where it is heated by radiation from the fuel region in a manner similar to that in other schemes[1] (see Fig. 1).

For the fuel loss rate from the wall region to be a minimum, the influence of the mixing action from turbulence, diffusion, and the entrainment of the fuel gas by the propellant flow

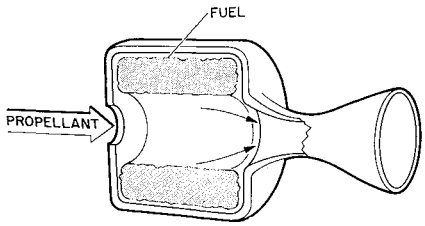

Fig. 1 Gas core nuclear rocket concept.

must be reduced. The means proposed here for accomplishing this is to employ the separating effect created by the rotational motion of the fluid. From past studies on vortex flows,[2–5] it was noted that the most effective separation of a light and a heavy gas occurs in the portion of flow that resembles solid-body rotation. Consequently, it would appear that the present scheme would perform best with a flowfield that possesses solid-body-like rotation. One possible means of producing a flow that approaches this condition is to drive the rotating flow by a Lorentz force which acts on the gas in the vicinity of the cylindrical wall of the chamber. To obtain a sharp separation between gases, the rotating flow must not only reach a high velocity but must also be free of excessive turbulence. It is believed this can best be achieved if the electrical current is spread uniformly through a volume in the shape of a cylindrical shell rather than taking the form of a single spoke.

Thus, the objective of the present work is to produce a high speed solid-body rotation by electromagnetic means in a simulated gas core nuclear rocket chamber and to explore the effectiveness of this flow in achieving a separation between heavy and light gas species. Although several studies[6,7] have been made to predict theoretically the performance of similar MHD-driven rotating flow devices, no experiments have been reported.

Apparatus

Chamber Design

In an attempt to fulfill the aforementioned objectives, a design was employed in which the electrical current is oriented in the axial direction and the magnetic field in the radial direction, as shown schematically in Fig. 2. This configuration has selected rather than the radial current, axial field configuration often considered by other investigators for the following reasons. First, by using this configuration, the current and hence the driving Lorentz force can possibly be confined to the chamber perimeter. In addition, following the scheme of Shepard,[8] multiple electrodes can be more easily accommodated. This arrangement forces the electrical current to divide (at least in the vicinity of the electrodes) rather than to amalgamate into a single spoke. With this in mind, 16 pairs of thoriated-tungsten electrodes, each of which is connected in series with a 2 ohm ballast resistor, were located in a circumferential pattern in the ends of the cylindrical test chamber as shown in Fig. 3.

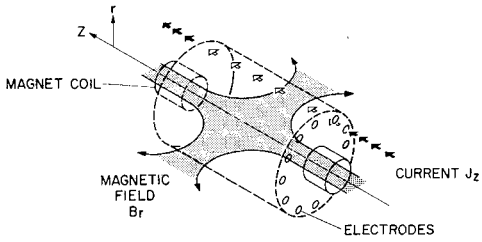

Fig. 2 Arrangement of current and magnetic field in the experimental apparatus.

The radial magnetic field is produced by two 400-turn coils of opposing polarity aligned with the axis of the test chamber, one coil being positioned at each end of the chamber. The diameter of the coils was chosen such that the radial magnetic field increases in strength to a maximum at a radius less than that of the electrode location and then decreases towards the cylinder wall. The motivation for sizing the magnetic field in this manner was derived from the results of prior tests with a preliminary apparatus in which the coil diameter was larger than the chamber diameter so the maximum field strength was reached at a radius outside the cylinder wall. It was found that the current in this case followed a path along the axis of the chamber rather than near the wall. Since, from Steenbeck's principle,[9] an electrical discharge will always choose a path and shape in which it will have a minimum dissipation of energy, it was hoped that the region of decreasing magnetic field near the cylindrical wall in the present design would provide a minimum energy path in the position desired for the discharge.

The cylindrical chamber encloses a volume of approximately one liter. The wall is constructed of copper rings electrically insulated from each other by boron-nitride disks. The cylinder ends are made of boron nitride and serve as a protection for the magnet coils that protrude into the cylinder a distance of 1.6 cm as illustrated in Fig. 3. The chamber is sealed and operates at pressures less than atmospheric. A mixture of xenon and helium is used to simulate the uranium-hydrogen mixture of a gas-core reactor. The helium is seeded with 4% hydrogen by volume for the purpose of spectroscopic diagnosis. The chamber is of a heat sink design with no cooling provided for the cylinder walls, magnet coils, or electrodes. Consequently, the tests are of short duration, typically less than 1 second. There is no inflow or outflow of gas from the chamber during a test. Although such a closed configuration does not correctly simulate a gas-core rocket, it was felt suitable for the limited objectives mentioned previously.

Instrumentation

Total current and voltage levels for the magnet and the electrical discharge are recorded as well as the individual currents to each electrode. In addition, information on rapid variations in the individual currents to four adjacent electrodes is obtained on two dual beam oscilloscopes. The oscilloscopes are triggered simultaneously so the sequential relationship among the current levels to these electrodes can be determined.

The pressure at the cylindrical wall of the chamber is measured through a pressure tap at the center section of the chamber. The pressure at the axis of the chamber is measured through a port which extends through the center of one of the

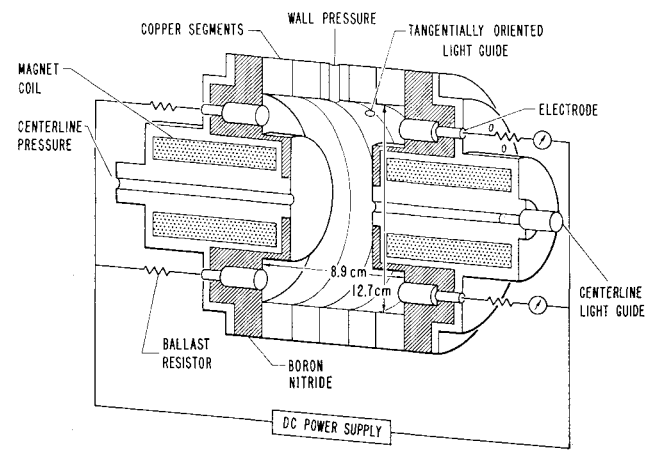

Fig. 3 Schematic cross section of the cylindrical chamber and electrical power hookup.

magnet coils to the end wall of the chamber. The pressures are sensed with strain gauge cells and are recorded on an oscillograph.

Information concerning the state of the plasma is obtained from the luminosity of the gas as detected by photomultiplier tubes through fiber optic light guides. One light guide is located so as to provide a view axially along the centerline of the chamber. Another provides a view of the region near the wall of the cylinder by looking tangentially inward through an orifice in the cylinder wall. The radiation emitted from these two regions is directed via light guides to two separate positions on the entrance slit of a spectroscope so that spectral lines from the two regions can be recorded simultaneously. The spectroscope employed is a Jarrell-Ash 2.25 meter Ebert model with a dispersion of 7.4 Å/mm and a span of 3600 Å. For several tests, spectral photographs were taken in the wavelength range of 4000 Å to 7600 Å to display the general qualitative features of the spectra. On all remaining tests, time-history spectral measurements were recorded for the purpose of determining the temperature and composition of the plasma in the two regions. To accomplish this, the intensities of the spectral lines 4671XeI, H_α, and H_γ emanating from the centerline region and the lines 4671XeI, H_α, and H_β from the wall region were simultaneously detected by six separate photomultiplier tubes. The 4671XeI line was detected by tubes with S-4 spectral response whereas the H_α, H_β, and H_γ lines were measured with tubes of S-20 response. On the basis of these line intensity measurements, a determination can be made of the change in concentration of the gases produced by the rotating flow.

Method of Operation

Prior to performing a test, the chamber is first evacuated and is then filled with the mixture of xenon and hydrogen-seeded helium. For most of the tests, the gas composition consisted of 56 mole percent xenon, 42.3 mole percent helium, and 1.7 mole percent hydrogen with an initial gas pressure in the chamber of either 12 or 16 torr. The operation of the device occurs in two steps. First, the discharge is initiated by drawing current from a constant-current d.c. power supply for a period of approximately 0.25 sec. At this point, while maintaining the same discharge current, the magnet is turned on to produce the J × B force for a duration of 0.25 to 0.35 sec. The magnet is powered by a separate d.c. supply. Although the tests were of relatively short duration, it was found that a pseduo-steady-state condition was reached during both the discharge-current-only period, i.e., the J-only period, and the J × B period, provided the run was of the smooth and stable category (this will be discussed later). Total discharge current varied between 400 and 2000 amps, and the radial component of the magnetic field at the maximum point between the centerline and the electrode location was in the range of 0.09–0.24 tesla, the field strength at the electrode location being approximately 85% of the maximum. The maximum power input to the gas that was encountered in these tests was approximately 200 kw.

Experimental Results

Current Path

As mentioned earlier, the effectiveness of the Lorentz forcel in driving the gas and the likelihood that solid-body-like rotation will be produced are dependent on the current path. On the basis of the current measurements for individual electrodes, it was found, that when the magnetic field was applied, the current would distribute evenly among the 16 electrodes.

The path of the electrical current through the gas within the cylinder was estimated from observations of the gas luminosity. Fig. 4 gives relative spectral line intensities from the gas as measured along the centerline of the chamber and near

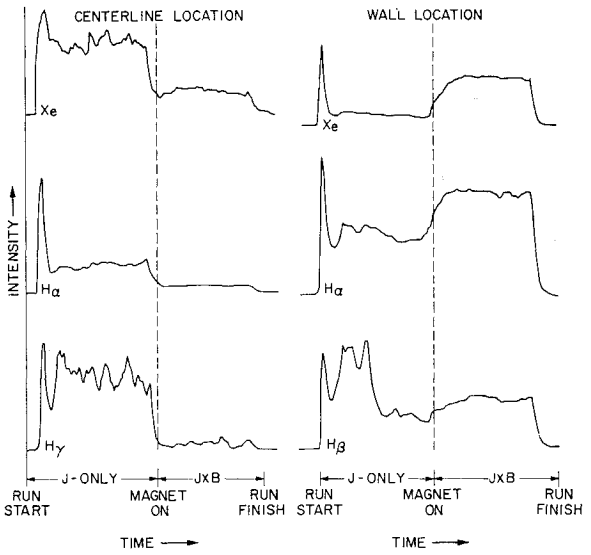

Fig. 4 Spectral line intensities from run 39; J = 1340 amp, B = 0.225 tesla, p_w/p_o = 2.3.

the wall of the chamber. The spectral lines shown in the figure demonstrate the basic response features that are typical of most of the runs although there tended to be variations in individual line response from run to run. Considering the response of the xenon line, it can be noted that the intensity is high at the centerline during the current-only portion of the run but decreases when the magnetic field is applied. Conversely, the intensity at the wall location, except for the peak at the start, is initially low but then increases as the magnetic field is applied. This behavior of the spectral line during the run can be attributed to a combination of two effects. The first of these is the increase in xenon concentration at the wall and the decrease at the center region under the influence of the gas rotation. The other effect that would lead to this behavior is a variation in the gas luminosity produced by a change in current path from the centerline of the chamber to the wall region when the magnetic field is applied. The presence of this latter effect is substantiated by the behavior of the hydrogen spectral lines. In this case the effect of the gas rotation would tend to decrease the concentration of hydrogen at the wall. However, it is noted that the behavior of the H_α line intensity is very similar to that of the xenon line; i.e., the intensity increases at the wall and decreases at the centerline when the magnetic field is applied. This strongly suggests that the current path, and hence the luminosity, is moving from the centerline region to the wall. A similar pattern of behavior is exhibited by the H_γ line intensity at the centerline and, to a lesser extent, by the H_β line intensity at the wall. It will be noted that the H_β line intensity during the current-only period shows oscillations at a fairly high level and then drops to a lower level prior to the onset of the magnetic field. The reason for this behavior is not known but it may be due in part to fluctuations in the path or paths of the current around the centerline region. Evidence of such fluctuations is also found on the other line intensity measurements, e.g., H_γ at the centerline. The evidence of these fluctuations disappears under the stabilizing effect of the magnetic field.

Based on the results from the current measurements to individual electrodes and the behavior of the luminosity measurements, it was concluded that a reasonably even current distribution around the outer circumference of the chamber is present whenever the magnetic field is applied.

Behavior of the Discharge

The electrical current discharge exhibits what appears to be two different modes of operation. Evidence of the existence of these modes was obtained from the oscilloscope traces of the

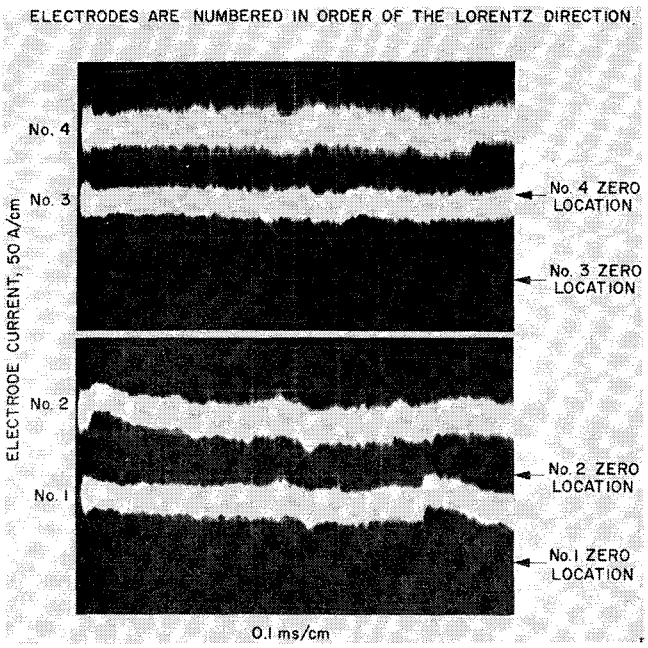

Fig. 5 Current to individual electrodes; J = 1200 amp, B = 0.23 tesla.

current to adjacent electrodes. In one mode, characterized by a fluctuation in the current at a frequency of the order of 1 MHz, the operation of the device was stable with essentially constant values for the discharge voltage and chamber pressures during both the J-only and J × B periods of the run. Oscilloscope traces of individual electrode current levels during the J × B period of the run are shown in Fig. 5 for this stable mode of operation. The mean current level per electrode is approximately 75 amperes and the amplitude variation of the disturbances is ±35%. It is believed that the current mode as illustrated by Fig. 5 may represent a reasonably uniform distribution of current. This belief is based on the fact that no high-amplitude oscillations in current are observed such as would exist[10] if moving spokes were present.

In the other discharge mode, the operation of the device was characterized by a sharp, continuous rise in the discharge voltage, pressure, and luminosity within the chamber during the J × B period of the run. These effects were accompanied by considerable heating of the chamber wall. Oscilloscope traces of the electrode currents during this mode of operation are shown in Fig. 6. The current patterns show severe oscillations at frequencies ranging between 10 kHz and 25 kHz and amplitudes which can exceed ±100% of the mean. In the worst cases, where the amplitude of the oscillations increased to large values, the operation of the device was quite unstable, and showed the sharp increase in measured values as mentioned above. It appeared that this discharge mode would occur either when contaminants were present in the chamber or when the chamber has inadvertently filled with an excess of helium to a much higher (above 40 torr) pressure than usual. A definite similarity in the pattern of the current traces for adjacent electrodes can be noted for this mode. The patterns show a phase shift between electrodes which appears to indicate motion of the current in the direction of the Lorentz force. It is believed that the current pattern exhibited in this mode is caused by a multiplicity of arc spokes rotating in the flow direction at a velocity ranging from 500 to 1500 m/sec.

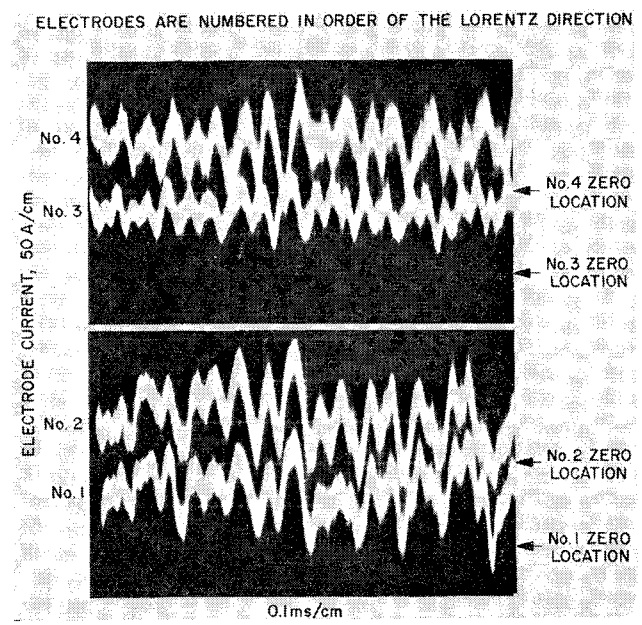

Fig. 6 Current to individual electrodes; J = 1250 amp, B = 0.224 tesla.

Gas Rotation

One of the primary objectives of this study was to produce a substantial rotational motion of the gas through the use of the Lorentz force. In the experiments carried out, the rotation of the gas was evaluated by measuring the pressure at the cylinder wall and at the centerline of the chamber. The pressure distribution within the chamber is related to the rotational velocity through Eq. (A4). Thus, when rotational motion of the gas is present there will be an increase in the wall pressure and a decrease in the centerline pressure. This behavior was observed in the present tests as shown by the typical pressure measurements in Fig. 7.

In general, the rotational velocity is a function of the radial temperature distribution and the species concentration dis-

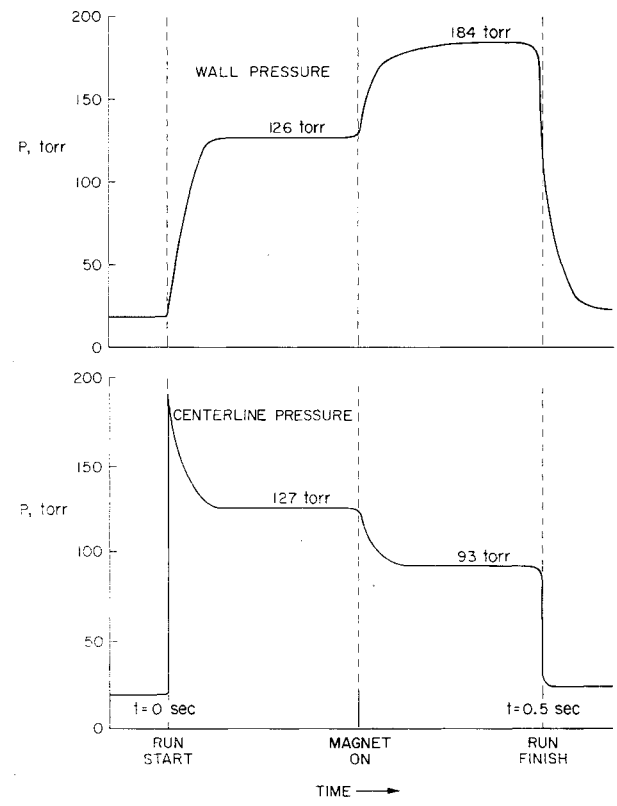

Fig. 7 Typical pressure time histories at the chamber wall and at the centerline; J = 1460 amp, B = 0.23 tesla.

tribution as well as the pressure gradient. These effects are included in the analysis of Appendix A. The resulting expression, given by Eq. (A18), is used to calculate the Mach number of the rotating gas.

The measured values of wall-to-centerline pressure obtained from the present tests are plotted in Fig. 8 as a function of the product of the magnetic field and total discharge current which is proportional to the Lorentz force. As seen from the figure, the pressure ratio seems to increase steadily with the Lorentz force, the maximum value attained being about 2.9. As indicated in the typical test data shown in Table 1, the temperature near the wall is found to be higher than that at the center by approximately 20%. Under such a condition, the Mach number of the mixture corresponding to the maximum pressure ratio obtained is approximately 1.18, the Mach number for the xenon gas being about 1.35.

It will be noted that the tests performed with initial charging pressures of 16 torr and higher do not appear to give as large a pressure ratio for the same Lorentz force as the tests at 12 torr. As shown in Table 1, the value of the Reynolds number based on the velocity near the wall indicates that the flow is well into the turbulent regime. Consequently, the observed behavior cannot represent an effect of transition from laminar to turbulent flow. Furthermore, the small change in Reynolds number caused by differences in charging pressure is not sufficient to make an appreciable change in the wall shear stress. It is suspected, therefore, that pressure may be affecting the discharge behavior; i.e., that the discharge at higher pressures was not as effective in driving the gas as it was at lower pressures.

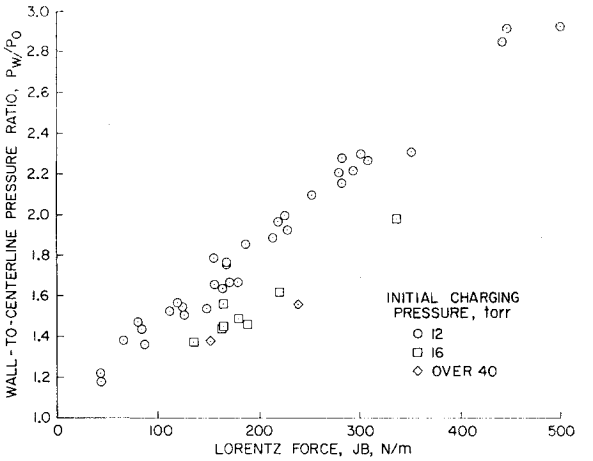

Fig. 8 Ratio of wall-to-centerline pressure as a function of Lorentz force.

Concentration Measurements

In order to determine whether or not the rotating flow produced by the test device developed a significant change in the relative concentration of the xenon and helium, spectroscopic measurements of composition were taken. Spectroscopic techniques for this purpose (e.g., Griem[11]) require that the plasma under observation be in chemical and electronic excitation equilibrium. These conditions were considered to be approximately valid in the present experiment because the neutral and electron densities are relatively high, the test time is much longer than the ionization and recombination times required for the gas to reach equilibrium, and the applied electric field is relatively small. In addition to the basic assumptions, the following conditions were assumed to apply: 1) the radiation from the gas consists only of the continuum from xenon and the xenon and hydrogen lines; 2) the plasma is optically thin to the measured radiation wavelengths; 3) the light-emitting medium is a slab with uniform properties along the line of observation; and 4) the mixture ratio of hydrogen to helium remains constant everywhere within the test chamber.

Assumption 4 is considered to be fairly accurate in the present test because the tangential Mach number of helium was always much smaller than unity. Consequently there will be no significant separation of hydrogen from helium due to the centrifugal force. In addition, the radial temperature change is not sufficient to cause an appreciable degree of thermal diffusion of hydrogen with respect to helium. The fixed ratio of hydrogen to helium was used to establish the helium concentrations based on the intensities of the hydrogen lines. This approach was taken since there was essentially no detectable radiation emitted by the helium under the conditions of the test.

While the other assumptions can be shown to hold approximately, assumption 1 is open to serious question. The reason for this is the possible presence of impurities within the chamber which could result in a substantial background spectrum. Whereas the continuum radiation from the xenon can

Table 1 Summary of typical test data—run 39

Test conditions	
Concentration ratio in chamber before test, Xe to He	1.3:1.0
Total pressure before test	12 torr
Total electric current	1340 amp
Voltage gradient	800 V/m
Total arc power	134 kw
Friction loss	31 kw
Radial magnetic field strength at electrode location	0.2 tesla
Pressure at cylinder wall during operation	133 torr
Pressure at cylinder centerline during operation	58 torr
State properties in centerline region	
Temperature	8200°K
Enthalpy	3100 J/gram
Degree of ionization of Xe	0.09
Electron density	0.5×10^{15} cm^{-3}

State properties in arc region	
Temperature	10,200°K
Enthalpy	4800 J/gram
Degree of ionization of Xe	0.44
Electron density	2.8×10^{16} cm^{-3}
Frozen sound speed for mixture	1.5 km/sec
(Frozen) Mach number for mixture	0.86
(Frozen) Mach number for Xe	1.05
Tangential velocity	1.29 km/sec
Electrical conductivity	3000 mho/m
Hall parameter	0.104
Interaction parameter based on circumference	1.9
Reynolds number based on diameter	1.1×10^5

be corrected for, there is no way to estimate on theoretical grounds the intensity of the radiation from unknown impurities in the wavelength bands where the spectral measurements were made in the present test. As is discussed later, spectral photographs of the radiation from the chamber did indicate the presence of some impurities and this may account for certain unexplainable behavior of the data.

Through the aforementioned assumptions, two relationships were developed to express the relative concentration of xenon to helium. They are the wall-to-centerline concentration ratio R_1 and the xenon dilution ratio at the center R_2:

$$R_1 = \frac{\text{xenon-to-helium ratio near wall}}{\text{xenon-to-helium ratio at centerline}} = \frac{(\bar{N}_{Xe}/N_{He})_a}{(\bar{N}_{Xe}/N_{He})_o} \tag{1}$$

$$R_2 = \frac{\text{xenon-to-helium ratio at center before magnetic field is applied}}{\text{xenon-to-helium ratio at center after magnetic field is applied}} = \frac{(\bar{N}_{Xe}/N_{He})_J}{(\bar{N}_{Xe}/N_{He})_{J\times B}} \tag{2}$$

Here $\bar{N}_{Xe}$ is the total xenon number density, i.e., the sum of the neutral and ionized xenon.

$$\bar{N}_{Xe} = N_{Xe} + N_{Xe^+} = N_{Xe} + N_e \tag{3}$$

The expression for R_2 involves the intensities of the 4671XeI and the H_α lines and the degree of ionization of the xenon whereas the expression for R_1 involves the intensities of these lines, the degrees of ionization for xenon, and the electron temperatures for the wall region and the centerline region. Since temperature effects are included in these expressions, this compensates for the fact that the discharge location shifts as the magnetic field is applied. The exact expressions for R_1 and R_2 and the details for developing these are given in Ref. 12.

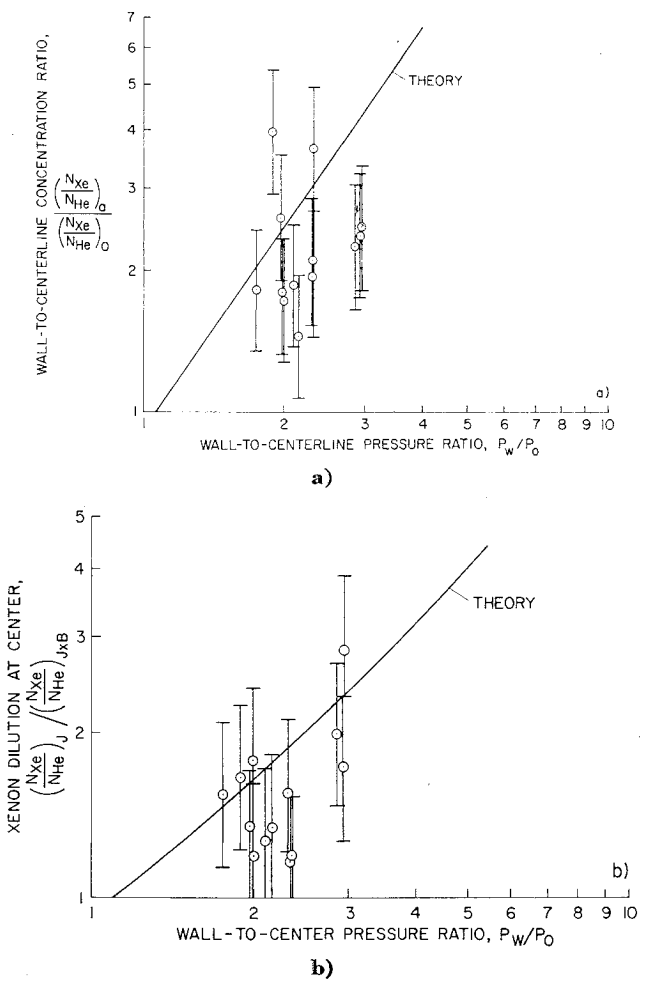

Fig. 9 Measured concentration ratio as a function of wall-to-center pressure ratio.

The electron temperature was determined at both the centerline and the wall region of the chamber during both the J-only and the J × B period of the run. In evaluating the spectroscopic data, the electron temperature could be determined to a first order from the ratio of the measured intensities of two hydrogen lines whose oscillator strengths are known exactly. To obtain a more accurate temperature, it was necessary to subtract from the measured line intensity the continuum background radiation at these wavelengths caused by the recombination of xenon ions. Because of uncertainties in the known values of the atomic constants involved in this correction, the resultant value for the temperature has an uncertainty of ±500°K. It might be noted that this uncertainty was reduced somewhat by virtue of the fact that a value for the oscillator strength of the 4671XeI line could be deduced from the test data. This permitted a cross-check on the calculation of the temperature correction due to continuum radiation.

Table 1 lists the properties of the plasma determined for a typical running condition. To arrive at these state properties it was necessary to make the additional assumption that thermal equilibrium exists in the plasma although this assumption is not required for determining the concentration ratios. The measured concentration ratios are shown in Figs. 9a and b and are compared with the theoretical values calculated by Eqs. (A18) and (A15). In the figures, the error bars indicate uncertainties caused by fluctuations in the line intensities during the run and the effect of the aforementioned uncertainty in the value for electron temperature. Both theory and experiment show a general trend of increasing separation as the rotation speed, evidenced by P_w/P_o, increases. Although there is a fair degree of scatter in the experimental data, the trend indicates clearly that significant species separation is achieved. At the highest pressure ratios produced, i.e., near P_w/P_o = 2.9, the degree of separation does not appear to be as great as at lower values of P_w/P_o. These runs correspond to a high-electrical discharge current, i.e., nearly 2000 amps. It may be that turbulence created by this relatively high current level acted to reduce the amount of species separation.

As mentioned earlier, the presence of impurities in the chamber may result in substantial background radiation over and above that from the xenon ions. The presence of excess background radiation affects the relative magnitude of the measurements for the H_β and H_γ lines and thus may lead to an overly high value for the electron temperature. This in turn leads to an overly high value for the ratio R_1. The experimental values that exceed the theory in Fig. 9a are probably in error because of this impurity effect. For the few tests in which spectral photographs were taken of the radiation from the chamber, only the lines of xenon and hydrogen were detected, for the most part, but in two instances the spectra showed many lines other than those of xenon and hydrogen. These lines, which in places were of such a number as to nearly resemble a continuum, were those belonging to tungsten, thorium, calcium, and sodium and appeared to originate from the electrodes and from the binder in the boron nitride insulator material.

It is suspected that the rather extensive scatter in the data for Fig. 9 may be a result of this background radiation from impurities. It was noted that erratic behavior in the line intensity measurements often occurred after the chamber had been disassembled, a process in which there is a good probability that contaminants can be introduced into the chamber. No provision was made in the present tests to measure the background radiation so its effect is unknown. However, in any future tests, steps will be taken to detect the background

radiation and to compensate for its effect on the spectroscopic measurements.

Discussion

As was pointed out earlier, the mode of current discharge plays an important role in attaining the conditions leading to the rotational motion best suited to produce an effective species separation. The best performance is believed to result when the discharge occurs uniformly. From the limited amount of information gathered in the present test, it is difficult to obtain an exact determination of the discharge behavior and current uniformity. As an example, there was an unianswered question as regards the effect of pressure on the nature of the discharge As seen in Fig. 8, the gas pressure affects the wall to centerline pressure ratio to a degree greater than expected from the change in the Reynolds number. There was evidence in the electric current records to suggest that the discharge tended to be spoke-like for the runs that deviate severely from the mean. Under these conditions, the measured pressure ratio and species separation were considerably reduced. Generally, however, the mode of discharge in the present test seems to be reasonably close to the desired condition.

Further evidence of a discharge mode favorable for effective acceleration was given by the low value of the Hall parameter $\omega\tau$ present in these tests (Table 1). This indicates the mechanism for acceleration will tend to be of a Faraday nature and will not be adversely affected by Hall effects. Also, a distinction was found between the present case and the case of a device with nonsegmented electrodes for the relationship between the applied discharge voltage and the magnetic field. Although not shown, the plot of applied discharge voltage vs magnetic field intensity indicates no sole dependency of the voltage on field strength in the present experiment. This differs from the case of the moving arc-spoke device in which the discharge voltage was found to depend almost entirely on the magnetic field strength for a given type of gas.[13] This implies that the gas in the present case is accelerated by a mechanism different from that which prevails in a rotating arc-spoke device.

In a prototype rocket, the exhaust gas would exit along the centerline of the cylinder. The mixture ratio of the heavy-to-light gas in the rocket exhaust would therefore correspond to that at the centerline in the present experiment. Calculations of the operating characteristics for such a rocket indicate that typically the device might operate with a propellant-to-fuel mass flow ratio of 50 and a rotational velocity corresponding to a Mach number for the fuel of about 2.5. Under these conditions the pressure within the chamber would be relatively low compared with other gas core concepts, i.e., on the order of 20 atm, and the diameter of the cavity would be relatively large, i.e., on the order of 6 m. The results from the present tests cannot be compared directly with these conditions for the prototype since a mixture heavily enriched with the heavy gas was used in the present tests instead of a light-gas-enriched mixture that is suited to the prototype. Such a deviation from the exact simulation was made in the interest of maintaining a relatively high electrical conductivity (which would result from the fissioning process in an actual gaseous core reactor).

The operating conditions for the prototype are limited by the convective heat-transfer rates to the cylindrical wall. To maintain these rates at reasonable levels, the rotational velocity must be restricted to values that cannot appreciably exceed the value mentioned previously. This, in turn, leads to relatively large cavity diameters in order to contain the required critical mass of fuel. To accommodate the severe heating conditions at the wall, transpiration cooling using part of the propellant would undoubtedly be required. However, even with transpiration cooling it is expected that a large fraction of the total fission energy would be transmitted to the cavity structure. Although part of this can be recovered in the propellant by regenerative cooling, the excess must be removed by means of a space radiator. The net result of this is a reduction in the thrust level at which the rocket can operate. Taking into account the weight of the space radiator, it is estimated that the thrust-to-weight ratio for a prototype rocket would be of the order of 0.01 and that the thrust level would be on the order of 40,000 kg. A rocket engine with such a thrust (but with a large specific impulse) might serve as an intermediate between the solid-core nuclear rocket and an electrical propulsion device. An estimation of the electrical power necessary to overcome the wall friction and maintain the rotational motion in such a rocket shows that the power is relatively nominal compared to the total fission power, i.e., on the order of 2%. It is within the capability of the system to obtain this power by employing a turbo-electric generator system operated by the propellant with the heat energy recovered from the cavity structure.

The present test does not correctly simulate a prototype gas-core rocket on the following two points. First, unlike a real rocket, there was no flow through the system. The effect of the through-flow is unknown at present, and awaits an additional investigation in the future. Secondly, in a prototype, the fuel gas will be multiply ionized and thus will behave as a uniform conducting medium, whereas in the present test, the ionized region is somewhat localized. Because of this difference, it is believed that the problems associated with the current discharge will be less in an actual gas-core rocket. Thus, the possible adverse effect of increased pressure on the performance indicated in Fig. 8 would diminish in a prototype rocket.

Conclusions

The Lorentz force developed by an axial current-radial magnetic field device is capable of producing a rotational motion of the gas to a Mach number in excess of 1. At the maximum Lorentz force applied, the velocity of the rotating gas flow produced a pressure at the chamber wall three times that at the centerline. For the mixture of xenon and helium tested, the concentration ratio of xenon to helium near the chamber wall was increased to a level approximately three times that near the center of the chamber. The current-field configuration used in the experiment is acceptable as a means of producing the desired condition for an effective gas separation. That is, the discharge current is distributed throughout the region near the chamber wall so as to produce a high-speed, solid-body-like rotation free of excessive turbulence.

Appendix A: Theoretical Characteristics under Ideal Conditions

In order to estimate the performance of the tested device, a theoretical analysis of the flow is made under the assumption of an ideal condition. The general picture of the flow field is shown schematically in Fig. 10. As shown in Fig. 10, the flow is confined in a cylinder, and is described by an r,θ coordinate system. The velocity components in the r and θ directions are u and v, respectively. All properties are steady and axially symmetric and hence are functions of r only. There is no mean flow motion in the r direction. The gas contained in the cylinder is a mixture of a monatomic heavy, fuel gas and monatomic light, propellant gas designated by the subscripts f and p, respectively. A small fraction of f-species is singly ionized. The electric current and magnetic fields are oriented in the axial and radial directions, as in the tested device.

The following are the major assumptions made for the purpose of simplifying the analysis. 1) The flow is purely two-dimensiional, i.e., the cylinder is infinitely long. 2) The electrical current passes through the infinitesimally thin layer of cylindrical shape located at $r = r_a$. 3) The flow is laminar in the region $0 \leqslant r < r_a$. 4) The mixture gas is thermody-

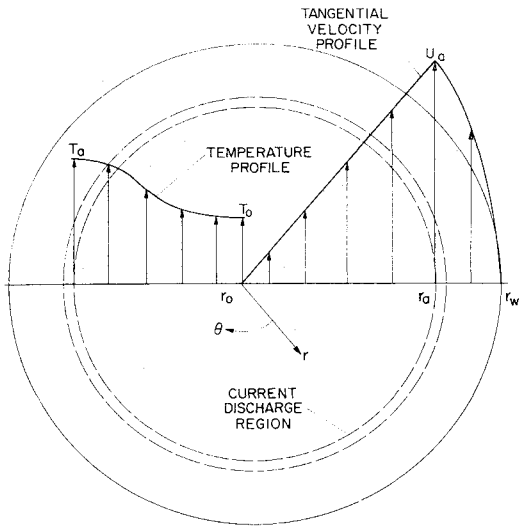

Fig. 10 Axial cross section of cylindrical chamber showing schematically the temperature field and velocity field.

namically in equilibrium everywhere within the cylinder. 5) The radial distribution of temperature is described by

$$T/T_o = 1 + A(r/r_a)^2 - \tfrac{1}{2}A(r/r_a)^4 \tag{A1}$$

where

$$A \equiv 2[(T_a/T_o - 1)] \tag{A2}$$

Here T_a is the temperature at $r = r_a$ and T_o is temperature at $r = 0$. The symmetrical temperature distribution, with zero slope at both $r = 0$ and $r = r_a$, qualitatively satisfies the physical requirements of the problem and was adopted as a reasonable guess of the actual profile. 6) The ion-electron pair of the f-species diffuses into the p-species with the same diffusion velocity as the neutral f-species. This assumption is the same as in Fay and Kemp.[14]

Under the preceding assumptions, the basic equations of motion reduce to the following for the region $0 \leqslant r < r_a$:

continuity:

$$\rho u r = \text{const} \equiv 0 \text{ (trivial)}$$

tangential momentum:

$$\frac{d}{dr}\left[\mu\left(\frac{dv}{dr} - \frac{v}{r}\right)\right] + \frac{2\mu}{r}\left(\frac{dv}{dr} - \frac{v}{r}\right) = 0 \tag{A3}$$

radial momentum:

$$\rho v^2/r = dP/dr \tag{A4}$$

where ρ is density, P is pressure, and μ is viscosity.

The equation of conservation of species is simplified because of assumption 6. Under assumption 6, the 4-component mixture can be treated as a binary mixture of f- and p-species. From Ref. 15, one derives the conservation equation as

$$\frac{D}{Dt}\left(\frac{\bar{N}_f}{\rho}\right) = \frac{1}{r}\frac{d}{dr}\left\{r\frac{N^2 m_p}{\rho}D_{fp}\left[\frac{d}{dr}\left(\frac{N_p}{N}\right) + \frac{\bar{N}_f N_p(m_f - m_p)}{\rho N}\frac{d\ \ln P}{dr}\right] - r\frac{D_f{}^T}{m_f}\frac{d\ \ln T}{dr}\right\} = 0 \tag{A5}$$

In Eq. (A5), m_f and m_p are the mass of the f-atom and p-atom, respectively, D_{fp} and $D_f{}^T$ are the binary diffusion coefficient and thermal diffusion coefficient concerned, and $\bar{N}_f$ and N are particle number densities defined by

$$\bar{N}_f = N_f + N_f{}^+ \tag{A6a}$$

$$N = N_f + N_f{}^+ + N_p \tag{A6b}$$

Because the concentration of the p-species is related to that of the f-species by the total mass conservation law, it is not necessary to write a conservation equation for the p-species separately. Further, the energy equation is not necessary because the temperature distribution is already specified by Eq. (A1). The boundary conditions for Eqs. (A3) to (A5) are

$$v = 0, \quad \bar{N}_f = (\bar{N}_f)_o \quad \text{at} \quad r = 0 \tag{A7a}$$

$$v = v_a \quad \text{at} \quad r = r_a \tag{A7b}$$

It should be noted here that Eqs. (A3) to (A5) apply only in the region $0 \leqslant r < r_a$. In the narrow region $r_a \leqslant r \leqslant r_w$, the presence of strong turbulence makes the assumption of laminar flow invalid, and therefore no attempt is made to analyze this region.

The solution of Eq. (A3) satisfying the boundary conditions (A7a, b) is simply

$$v = v_a(r/r_a) \tag{A8}$$

That is, the flow has the pattern of a solid-body rotation in the region $0 \leqslant r < r_a$.

By the use of Eq. (A8), one can now integrate Eq. (A5). To do this, one substitutes Eq. (A8) first into the left-hand side of Eq. (A4). The resulting expression for dP/dr is then substituted into Eq. (A5). Then, defining the f-species concentration C as

$$C \equiv \bar{N}_f/N \tag{A9}$$

and the frozen speed of sound of the f-species, c_f, by

$$c_f = (1.66P_f/\rho_f)^{1/2} \tag{A10}$$

the species mass conservation equation becomes approximately

$$r_a\frac{dC}{dr} - 1.66\frac{v_a{}^2}{c_f{}^2}\frac{r}{r_a}(1 - C)C = -\frac{\rho D_f{}^T r_a}{m_f m_p N^2 D_{fp}}\frac{d\ \ln T}{dr} \tag{A11}$$

in which m_p is neglected in comparison with m_f.

From Ref. 15, one finds that there exists an approximate relationship between $D_f{}^T$ and D_{fp}

$$\rho D_f{}^T/m_f m_p N^2 D_{fp} \simeq 0.4C(1 - C) \tag{A12}$$

Substituting Eq. (A12) into Eq. (A11), and neglecting the concentration of electrons in comparison with that of heavy particles, one obtains

$$r_a\frac{dC}{dr} - \left[1.66M_{fa}{}^2\frac{T_a}{T_o}\cdot\frac{T_o}{T}\frac{r}{r_a} - 0.4r_a\frac{d}{dr}\ln\frac{T}{T_o}\right]\times(1 - C)C = 0 \tag{A13}$$

in which M_{fa} is the Mach number of the f-species based on the frozen sound speed c_f taken at $r = r_a$

$$M_{fa} = (v/c_f)_a \tag{A14}$$

Because T/T_o in Eq. (A13) is given explicitly by Eqs. (A1) and (A2), Eq. (A13) can be integrated, the result being

$$C = C_o F(A, r/r_a, M_{fa}{}^2)/[1 - C_o + C_o F(A, r/r_a, M_{fa}{}^2)] \tag{A15}$$

in which

$$F \equiv \left[\frac{(2A + A^2)^{1/2} + A}{(2A + A^2)^{1/2} - A}\cdot\frac{(2A + A^2)^{1/2} - A(1 - r^2/r_a{}^2)}{(2A + A^2)^{1/2} + A(1 - r^2/r_a{}^2)}\right]^{(1+A/2)/(2A+A^2)^{1/2}(1.66M_{fa}{}^2/2)} \frac{1}{[1 + A(r/r_a)^2 - (A/2)(r/r_a)^4]^{0.4}} \tag{A16}$$

and C_o is the value of C at $r = 0$.

With C known, one can now find the pressure distribution. To find the pressure, one first writes density ρ in the form

$$\rho = \rho_o\{[1 - (m_p/m_f)]C + (m_p/m_f)\}/\{[1 - (m_p/m_f)]C_o + (m_p/m_f)\} \quad \text{(A17)}$$

ρ_o being the value at $r = 0$. By substituting Eq. (A17) into (A4) and integrating, one obtains

$$\frac{P}{P_o} = 1 + \frac{(1.66/2)(T_a/T_o)M_a^2}{[1 - (m_p/m_f)]C_o + (m_p/m_f)} \times \left[\frac{1}{r_a^2}\left(1 - \frac{m_p}{m_f}\right)\int_0^{r^2} Cd(r^2) + \frac{m_p}{m_f}\frac{r^2}{r_a^2}\right] \quad \text{(A18)}$$

Here M_a is the Mach number based on the frozen sound speed of the mixture

$$M_a \equiv (v/c)_a \quad \text{(A19)}$$

and

$$c \equiv (1.66P/\rho)^{1/2} \quad \text{(A20)}$$

Because C is given explicitly in Eq. (A15), Eq. (A18) can be evaluated by quadrature using a computer.

The approximate behavior of the species concentration and pressure distribution will now be investigated. The species separation ratio between the center of the cylinder and the region near the cylinder wall can be defined, and found from Eq. (A15), as

$$\frac{(\bar{N}_f/N_p)_a}{(\bar{N}_f/N_p)_0} \equiv \frac{C_a/1 - C_a}{C_o/1 - C_o} = \left(\frac{(2A + A^2)^{1/2} + A}{(2A + A^2)^{1/2} - A}\right)^{(1+A/2)/(2A+A^2)^{1/2}\cdot 1.66M_{fa}^2/2)} \times \left(\frac{T_o}{T_a}\right)^{0.4} \quad \text{(A21)}$$

The function

$$\left(\frac{(2A + A^2)^{1/2} + A}{(2A + A^2)^{1/2} - A}\right)^{(1+A/2)/(2A+A^2)^{1/2}}$$

is weakly dependent on the temperature ratio T_a/T_o. In particular, for a constant temperature case $T_a/T_o = 1$ the species separation ratio becomes

$$(\bar{N}_f/N_p)_a/(\bar{N}_f/N_p)_o \to \exp(1.66/2)M_{fa}^2 \quad \text{(A22)}$$

Thus, it is seen that the species separation ratio is mainly a function of the Mach number of the f-species at the peak velocity station $r = r_a$.

In a similar but more complicated way, one can show that, for the constant temperature case, the pressure ratio can be approximated by

$$P_a/P_o \to \exp(1.66/2)M_a^2 \quad \text{(A23)}$$

That is, the pressure ratio is determined by the Mach number of the gas mixture. Using the approximate relationship

$$M^2/M_f^2 = C + (1 - C)(m_p/m_f) \simeq C$$

one finds that the species separation ratio and the pressure ratio are related approximately by

$$(N_f/N_p)_a/(N_f/N_p)_o \simeq (P_a/P_o)^{1/C_a} \quad \text{(A24)}$$

where C_a is the value of C at $r = r_a$.

One can also increase the separation ratio by decreasing the relative concentration of the f-species at r_a. However, because the absolute concentration of the f-species must not be less than the critical value required for a sustained fission chain reaction, the reduction in C_a can be achieved only by increasing the absolute partial pressure of the propellant gas, resulting in an increase in the structural strength requirements. Because a C_a value of approximately 0.2 is considered to be the minimum admissible[16] from the structural point of view, and also because a species separation ratio of at least 500 is assumed to be required for the present separation scheme to be useful, the minimum pressure ratio necessary for possible utilization of this scheme is approximately

$$(P_a/P_o)_{\text{min req}} = (500)^{0.2} = 3.46$$

References

[1] McLafferty, G. H., "Survey of Advanced Concepts in Nuclear Propulsion," *Journal of Spacecraft and Rockets*, Vol. 5, No. 10, Oct. 1968, pp. 1121–1128.

[2] Clark, J. et al., "Open-Cycle and Light-Bulb Types of Vortex-Stabilized Gaseous Nuclear Rocket," *Journal of Spacecraft and Rockets*, Vol. 5, No. 8, Aug. 1968, pp. 941–947.

[3] Pivirotto, T. J., "Mass-Retention Measurements in a Binary Compressible Vortex Flow," TR 32-864, June 15, 1966, Jet Propulsion Lab., Pasadena, Calif.

[4] Lewellen, W. S., Ross, D. H., and Rosenzweig, M. L., "Binary Diffusion in a Confined Vortex," *AIAA Journal*, Vol. 4, No. 3, March 1966, pp. 396–405.

[5] Keyes, J. J., Jr., "Experimental Study of Flow and Separation in Vortex Tubes With Application to Gaseous Fission Heating," *ARS Journal*, Sept. 1961, pp. 1204–1210.

[6] Romero, J. B., "Fuel Containment in the Gaseous-Core Nuclear Rocket by MHD-Driven Vortices," *AIAA Journal*, Vol. 2, No. 6, June 1964, pp. 1092–1099.

[7] Johnson, K. P., "A Plasma-Core Nuclear Rocket Utilizing a Magnetohydrodynamically-Driven Vortex," *AIAA Journal*, Vol. 4, No. 4, April 1966, pp. 635–643.

[8] Shepard, C. E., Watson, V. R., and Stine, H. W., "Evaluation of a Constricted-Arc Supersonic Jet," TN D-2066, 1964, NASA.

[9] Peters, T., "Bogenmodelle Und Steenbeck'sches Minimumprinzip," ("Arc Models and Steenbeck's Minimum Principle,") *Proceedings of the 5th International Conference on Ionization Phenomena in Gases*, Vol. 1, 1961, pp. 885–896. English translation by Ranson, H. C., Library Translation No. 1041, 1963, Royal Aircraft Establishment.

[10] Larson, A. V., "Experiments on Current Rotations in an MPD Engine," *AIAA Journal*, Vol. 6, No. 6, June 1968, pp. 1001–1006.

[11] Griem, H. R., *Plasma Spectroscopy*, McGraw-Hill, New York, 1964.

[12] Love, W. L. and Park, C., "An Experiment on the MHD-Driven Flow for a Gas-Core Nuclear Rocket," AIAA Paper 69-727, San Francisco, Calif., 1969.

[13] Guile, A. E. and Naylor, K. A., "Further Correlation of Experimental Data for Electric Arcs in Transverse Magnetic Fields," *Proceedings of the IEE*, Vol. 115, No. 9, Sept. 1968, pp. 1349–1354.

[14] Jay, J. A. and Kemp, K. H., "Theory of Stagnation-Point Heat Transfer in a Partially Ionized Diatomic Gas," *AIAA Journal*, Vol. 1, No. 12, Dec. 1963, pp. 2741–2751.

[15] Hirschfelder, J. O., Curtis, C. F., and Bird, R. B., *Molecular Theory of Gases and Liquids*, Wiley, New York, 1954, Chap. 8.

[16] Ragsdale, R. G., "Are Gas-Core Nuclear Rockets Attainable?" AIAA Paper 68-570, Cleveland, Ohio, 1968.